NJC

Fabrication of core-shell CoFe2O4@HAp nanoparticles: A novel magnetic platform for biomedical applications

Journal:	*New Journal of Chemistry*
Manuscript ID	NJ-ART-05-2019-002510.R1
Article Type:	Paper
Date Submitted by the Author:	23-Jul-2019
Complete List of Authors:	D, Karthickraja; Periyar University S, KARTHI; Henan University Gangadharan, Ajithkumar; University of Texas at San Antonio, Department of Physics and Astronomy; Manipal University; Texas Agriculture and Mechanical University Sardar, Dhiraj; University of Texas at San Antonio, Physics & Astronomy Martirosyan, Karen; University of Texas Rio Grande Valley, Physics G.C, Dannangoda; University of Texas Rio Grande Valley, Physics Girija, Easwaradas; Periyar University, Physics

SCHOLARONE™
Manuscripts

Fabrication of core-shell CoFe$_2$O$_4$@HAp nanoparticles: A novel magnetic platform for biomedical applications

D. Karthickraja[a], S. Karthi[b], G.A. Kumar[c,d,e], D.K. Sardar[c], G.C. Dannangoda[f], K.S.

Martirosyan[f], E.K. Girija[a]*

[a] Department of Physics, Periyar University, Salem 636 011, Tamil Nadu, India.

[b] College of Chemistry and Chemical Engineering, Henan University, Kaifeng 475004, China.

[c] Department of Physics and Astronomy, University of Texas at San Antonio, San Antonio, Texas 78249, USA

[d] Department of Atomic and Molecular Physics, Manipal University, Manipal 576 104, Karnataka, India.

[e] Department of Natural Sciences, Texas Agriculture and Mechanical University, One University Way, San Antonio, TX 78224

[f] Department of Physics and Astronomy, University of Texas at Rio Grande Valley, Brownsville, Texas 78520, USA

* Corresponding author. Tel.: +91 9444391733; Fax: +91 427 2345124

E-mail address: girijaeaswaradas@gmail.com (E. K. Girija)

Abstract

Core-shell CoFe$_2$O$_4$@HAp magnetic nanoparticles were successfully prepared by a simple two-step hydrothermal process, and the physicochemical and magnetic properties have been studied. X-ray diffraction patterns and Fourier transform infrared spectroscopy of the as-synthesized samples reveal that the nanoparticles are composed of both the phases (HAp@CoFe$_2$O$_4$). Core-shell formation was confirmed by TEM and from the magnetization studies using a vibrating sample magnetometer (VSM), the ferromagnetic nature of the synthesized core-shell nanoparticles at room temperature has been confirmed with a saturation magnetization (Ms) and coercivity values of 9.04 emu/g and 0.1 T, respectively. It has been observed that heat treatment enhanced the saturation magnetization when compared to the as-prepared samples. The

reason for this enhanced magnetic property after heat treatment is discussed based on the magnetic moment and anisotropy calculations. The potential cytocompatibility of the sample was confirmed by fibroblast 3T3 cells.

Key words: cobalt ferrite, hydroxyapatite, encasing, magnetic nanorods, ferromagnetic.

1. Introduction

Ferrite based magnetic nanoparticles such as Fe_3O_4, γ-Fe_2O_3, $NiFe_2O_4$, $CoFe_2O_4$, $ZnFe_2O_4$ and $MnFe_2O_4$ are being widely investigated for magnetic hyperthermia, magnetic drug delivery, non-invasive magnetic resonance imaging, electromagnetic wave absorption, energy storage applications *etc* [1–4]. Size dependence on the physicochemical properties of nanostructured ferrites is an important factor that dictates design engineering for specific applications. Among the various biomedical applications of magnetic nanoparticles, magnetic hyperthermia is an attractive mode of cancer therapy that can destroy tumor and cancer cells locally and selectively on application of an externally applied AC magnetic field using magnetic nanoparticle as the thermoseed. However, factors like the amount of magnetic nanoparticle used for the treatment and toxic effects of magnetic nanoparticles are some of the major concerns in the magnetic hyperthermia [5,6].

Magnetite is a widely suggested hyperthermia agent due to good cytocompatibility and superparamagnetic property. However, the challenge regarding magnetite is that it has poor magnetic property and less heating ability at small sizes and under physiological conditions [7,8]. Furthermore, specific absorption rate is an important parameter that can be related to the hysteresis loss of the magnetic nanoparticle. Several approaches have been suggested to improve the specific loss power of magnetic nanoparticle such as tuning of magnetic anisotropy, use of higher saturation magnetization materials [7,9], exchange-coupling *via* soft and hard magnetic phases [10], tailoring the size and shape of the magnetic nanoparticles [11] *etc*. It is well documented in the literature

that tailoring the shape of the magnetic nanoparticle from spherical to cubic [12], octapodes [6] and rods [13] improve the specific absorption rate *via* magnetic anisotropy.

Recently, cobalt ferrite magnetic nanoparticles is getting a lot of attention as an alternative to the well-known iron oxide owing to their excellent magnetic properties such as high magnetocrystalline anisotropy, large Curie temperature, moderate saturation magnetization even with small particle size. All these properties of cobalt ferrite helps to decrease the therapeutic concentration of the magnetic nanoparticle. Moreover, these magnetic properties can be easily tuned by tuning the size, shape and heat treatment at a suitable temperature [14,15]. Sumithra *et al* suggested the, possibility and potential use of cobalt ferrite nanoparticles for biomedical applications based on the reports over the past decades [8]. Robles *et al* reported the, core/shell exchange-coupled magnetite/cobalt ferrite nanoparticles for magnetic hyperthermia [10].

Designing of magnetic nanoparticle for biomedical applications demands surface modification to improve their effective biodistribution, hydrophilicity, colloidal stability and biocompatibility. Both organic and inorganic materials are under investigation as surface coating agents [2]. Among the inorganic materials studied, hydroxyapatite (HAp) is gaining much attention for wide biomedical applications due to its inherent biocompatible nature and analogy to the material component of bone and teeth of human being [5,16,17].

Previously we reported the coating of apatite over Fe_3O_4 (FAp) and $NiFe_2O_4$ (HAp) *via* a two steps process [18–20]. In one of the approaches HAp matrix was doped with Fe and Ni ions by wet precipitation followed by heat treatment for 2 h which yielded micron-sized $NiFe_2O_4$ embedded apatite with which hyperthermia temperature was achieved in less than 2 min. using 30 mg of the sample [19]. In a modified approach Fe and Ni ions doped HAp nanoparticles was prepared *via* organic modifier mediated hydrothermal synthesis followed by rapid thermal

processing. This yielded novel nanosized apatite coated $NiFe_2O_4$, yet achieving hyperthermia temperature with 10 mg/ml in 10% PEG solution even after 10 min magnetic field exposure was a challenging task [20]. While, nanoscale biocompatible HAp matrix embedded magnetic nanoparticle with essential factors such as high saturation magnetization and magnetic anisotropy (coercivity) are required for attaining therapeutic temperature in a relatively shorter time.

Hence an attempt has been made to prepare core-shell structured $CoFe_2O_4$@HAp magnetic nanoparticles as an accessible/promising candidate for magnetic hyperthermia. In this manuscript, we describe a simple two-step process to fabricate HAp coated cobalt ferrite magnetic nanoparticles with improved saturation magnetization achieved *via* heat treatment.

2. Experimental procedure

2.1. Chemicals

Analytical grade calcium nitrate tetrahydrate $[Ca(NO_3)_2.4H_2O]$, diammonium hydrogen phosphate $[(NH_4)_2HPO_4]$, iron (III) nitrate nonahydrate $[Fe(NO_3)_3.9H_2O]$, cobalt (II) nitrate hexahydrate $[Co(NO_3)_2.6H_2O]$, sodium hydroxide [NaOH] and ammonia solution $[NH_4OH]$ were procured from Merck and used without any further purification. Double distilled water was employed as the solvent.

2.2. Synthesis of core-shell magnetic nanoparticles

Step 1. 0.25 M of $Co(NO_3)_2.6H_2O$ and 0.5 M of $Fe(NO_3)_3.9H_2O$ solutions were prepared and mixed. 3 M of NaOH was added to the above mixture and stirred for 1 h at 80 °C. Dark black precipitate (pH above 11) was obtained and transferred into Teflon lined autoclave reactor which was then subjected to hydrothermal treatment at 120 °C for 2 h. Then the obtained precipitate was washed several times with double distilled water, and the resultant product was dried at 100 °C for 4 h, and the sample was named as A.

Step 2. 0.2 g of synthesized sample A was mixed in 0.1 M of $Ca(NO_3)_2\,4H_2O$ solution. To this 0.06 M of $(NH_4)_2HPO_4$ solution was added dropwise, and then the mixture was subjected to ultrasonication assisted mechanical stirring for 1 h while maintaining the pH above ten by adding NH_4OH solution. The obtained precipitate was transferred into a Teflon lined autoclave reactor and subjected for hydrothermal treatment at 120 °C for 2 h. Then the precipitate was washed several times with double distilled water followed by freeze-drying, and this sample was named as B. Product B was held isothermally at 800 °C for 1 h (Muffle Furnace, NSW103) and then cooled naturally to the room temperature. This heat treated sample was named as C. Similarly, for comparison purpose sample A was also heat-treated at 800 °C for 1 h.

2.3.   Characterization

The X-ray diffraction (XRD) patterns of synthesized samples were obtained using Rigaku MiniFlex - II powder X-ray diffractometer in the 2θ range 20-65 degree with CuKα radiation (1.5406 $\mathring{A}$). The average crystallite size of cobalt ferrite was calculated from (311) plane of XRD pattern using Scherrer's approximation [21]

$$D_{hkl} = \frac{K\lambda}{\beta\,cos\theta} \qquad\qquad (1)$$

Where, D_{hkl} is the average crystallite size, λ is the wavelength of the CuKα radiation, K is broadening constant ($K = 0.9$), β is the full width at half maximum (in radian) and θ is the diffraction angle (degree) [19]. The X-ray density of cobalt ferrite was calculated using the following equation,

$$\rho_X = \frac{8\,M}{N_A a^3} \qquad\qquad (2)$$

where, M, N_A and a are the molecular weight (in g/mol), Avogadro's number (6.022×10^{23} mol^{-1}) and lattice constant respectively [22].

The functional groups present in the samples were analyzed using a Perkin Elmer RXI Fourier transform infrared (FTIR) spectrometer in the region of 4000-400 cm^{-1} with a 4 cm^{-1} resolution by KBr pellet technique. The morphology and elemental mapping of the samples was examined using high-resolution transmission electron microscopy (HR-TEM), JEOL JEM-2100, Japan and Phillips Tecnai TEM. The magnetic properties of the samples were determined by Physical Property Measurement System (PPMS EverCool-2, Quantum Design, Inc.) using vibrating sample magnetometer (VSM) option. Hysteresis loops (M-H) were measured in the field range -9 to +9 T at 300 K. Coercivity (H_C) and saturation magnetization (M_S) were estimated from the *M-H* curves. The magnetic moment (*m*) per formula unit (in μ_B) of the samples were calculated using the relation

$$m = \frac{M_S \times M_W}{5585} \tag{3}$$

where, M_W is molecular weight of cobalt ferrite (in g/mol), M_S is saturation magnetization magnetization of cobalt ferrite (in emu/g) and 5585 is the magnetic factor [23].

The first order cubic magnetocrystalline anisotropy constant (K_1) of the samples was estimated using the law of approach to saturation (LAS) in the high field region; the law designates the dependence of magnetization (*M*) on the applied field (*H*) for $H \gg H_C$. According to the law of approach to saturation, the magnetization as a function of the applied magnetic field is

$$M = M_S\left(1 - \frac{b}{H^2}\right) + \kappa H \tag{4}$$

$$b = \frac{8 K_1^2}{105 \mu_0^2 M_S^2} \tag{5}$$

$$K_1 = \mu_0 M_S \sqrt{\frac{105 \times b}{8}} \tag{6}$$

where, b is correlated with magnetocrystalline anisotropy constant (K_1), M, M_S, and H the magnetization, saturation magnetization and applied magnetic field (in A/m) respectively. μ_0 is the permeability of free space (1.257×10^{-6} mKg S^{-2}A^{-2}). The numerical constant 8/105 is the cubic anisotropy of random oriented polycrystalline materials [24]; K_1 is the cubic magnetocrystalline anisotropy constant (J/m^3); κH is forced magnetization term and κ is the high temperature susceptibility with high field. Generally forced magnetization term is zero at room temperature (300 K) [24–28]. Hence M_S and b are the fitting parameters in Equation 4.

Cytocompatibility assay

The cytotoxicity of the sample C was tested with fibroblast 3T3 cells using MTT (3-(4,5-dimethylthiazol-2-yl)-2,5-diphenyltetrazolium bromide tetrazolium) assay. The cells were cultured with 10 % fetal bovine serum (FBS) and antibiotics (100 µg/ml penciline and 100 U/ml streptomicine) at 37 °C under humidified atmosphere of 5 % CO_2 and 95 % air. The cultured cells were seeded at density of 10^5 cells per ml in 96 well plate followed by incubation for 24 h followed by sample C was added to the culture medium at different concentrations (50, 100, 200, 300, 400 and 500 µg/ml) and then incubated for further 24 h at 37 °C in 5 % CO2 and 95 % air and 100 % relative humidity. After an incubation time of 24 h, 15 µl of MTT reagent (5 mg/ml) in phosphate buffered saline was added to each well and further incubated at 37 °C for 4 hrs. After, MTT supernatants was discarded, the dark formazan crystals were dissolved in 100 µl of dimethyl sulfoxide and measure optical density (OD) using microplate reader. The percent (%) of cell viability was calculated using Eqn. 7.

$$Cell\ viability\ (\%) = \left(\frac{OD_{Sample\ C}}{OD_{Control}}\right) \times 100 \dots\dots\dots\dots (7)$$

Where, $OD_{Sample\ C}$ is the optical density of cells cultured with sample C and $OD_{Control}$ is optical

density of cells without sample.

3. Results and Discussion
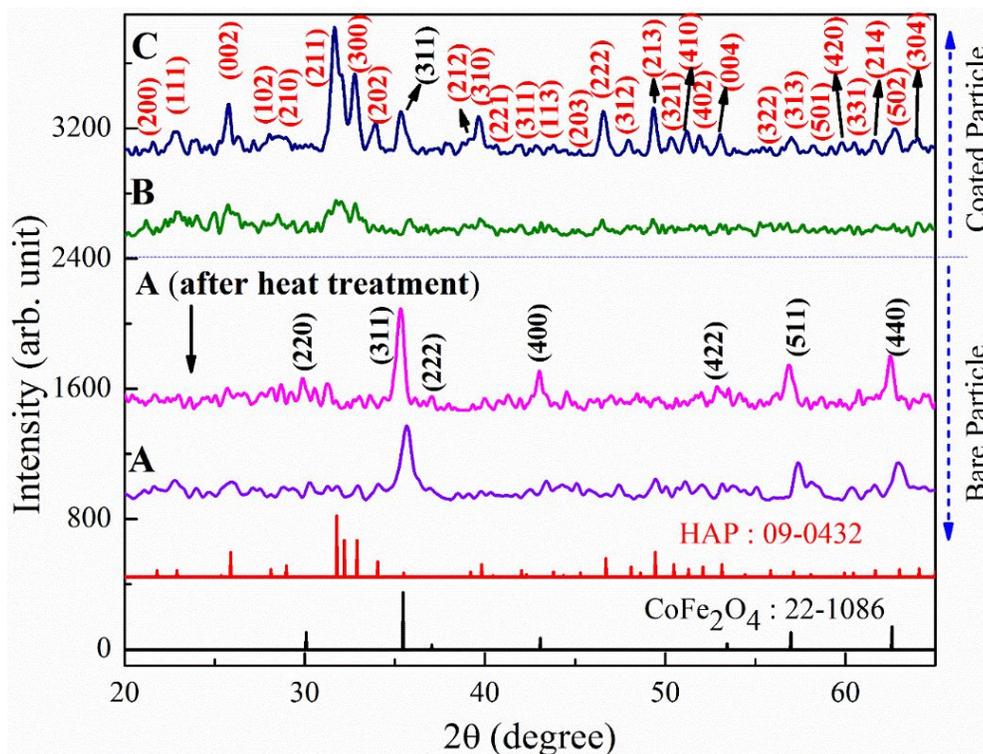
Fig. 1. X RD patterns of synthesized samples before and after heat treatment along with the JCPDS data of CoFe$_2$O$_4$ and HAP. The *y*-axis is appropriately scaled for comparison purpose.

The XRD patterns of the synthesized samples are shown in Fig. 1.   It is obvious that the

XRD pattern of sample A matches with the standard JCPDS card for cobalt ferrite (22-1086) with

a cubic unit cell structure [29] . The broad diffraction peaks suggest the existence of nanosized

crystals and the less crystalline nature of the sample. Heat treatment significantly improved the

crystallization of sample A as can be observed from the XRD pattern. The calculated lattice

constant, unit cell volume, X-ray density and crystallite size of the cobalt ferrite are given in Table

1. The XRD pattern of sample B did not reveal any resolved intense diffraction peaks of both HAp

and cobalt ferrite phases. Heat treatment of B resulted in resolved intense peaks of both the phases

(HAP-JCPDS card No. 09-0432 [16] and $CoFe_2O_4$) revealing the enhancement in crystallinity as

seen in sample C.

Phase pure HAp is known to be thermally stable up to 1400 °C [30]. But, preparation

condition, ionic substitution *etc* can affect the thermal stability of HAp nanoparticles leading to

phase transition. In the present study after heat treatment, sample B did not show the presence of

any other calcium phosphate phases. Ultrasonic irradiation and freeze drying adopted for the

synthesis of the sample might have enhanced the thermal stability of the HAp nanoparticles [31].

Table 1. Lattice constant, unit cell volume, x-ray density and crystallite size of the cobalt ferrite deduced from XRD

Sample code	Lattice constant (Å)	Unit cell volume (Å)^3	X-ray density (g/cm^3)	Crystallite size (nm)
A	8.347	581.5	5.357	31.6
A (after heat treatment)	8.424	597.7	5.151	40

The FTIR spectra of samples are shown in Fig. 2. The FTIR spectrum of sample A shows

strong broadband at 598 cm^{-1} which is due to the intrinsic Co-O stretching vibration which

indicates the existence of spinel ferrite. The peaks around 950 and 1155 cm^{-1} are attributed to the

Fe-Co alloy system [32,33]. The band at 1384 cm^{-1} is ascribed to the symmetric vibration of NO_3^-

group. The O–H stretching vibrations are observed at 3410 and 2922 cm^{-1}, the absorption band

present at 1625 cm^{-1} is due to bending of the absorbed water molecules [34,35]. The FTIR spectra

of sample B have characteristic PO_4^{3-} (v_4) vibrations of HAp at 566 and 603 cm^{-1} along with other

phosphate peaks at 473 (v_1), 963 (v_2) and 1037 (v_3) cm^{-1}. The bands at 3573 and 632 cm^{-1} are the

characteristic O-H stretching vibrations of HAp. The stretching and bending modes of adsorbed

water molecules are observed at 3423 and 1639 cm^{-1}, respectively. The peaks around 873, 1423

and 1456 cm^{-1} correspond to the CO_3^{2-} ions which might have got incorporated in to the sample

due to the reactive absorption of atmospheric carbon dioxide by the sample during the sample

preparation [16,36]. The $CoFe_2O_4$ peaks could not be distinguished since the characteristic Co-O

band at 598 cm^{−1} overlapped with the phosphate peaks of HAp. The peaks due to adsorbed water

and carbonate molecules disappeared in sample C because of heat treatment.
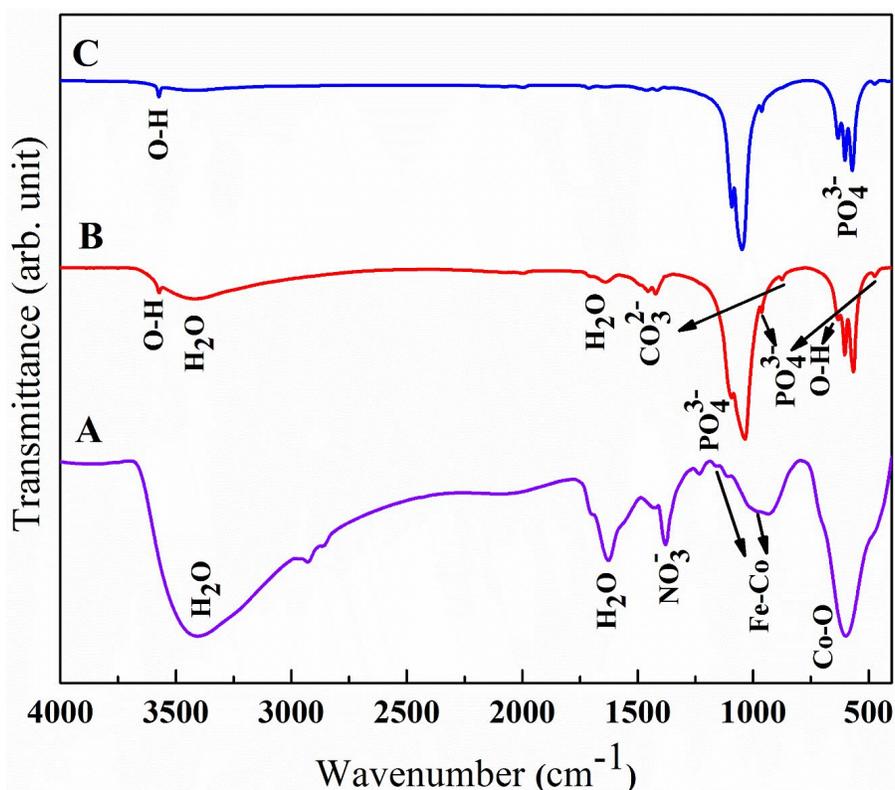
Fig. 2. FTIR spectra of synthesized samples A) as prepared cobalt ferrite, B) as prepared coated sample and C) heat treated coated sample.

The TEM image of sample A shown in Fig. 3 (a) reveals nanoparticles with dual

morphologies like spherical (red-arrow) and rhombohedral (green-arrow). Hydrothermal method

is a novel technique to produce nanoparticles with controlled size and shape by governing the

reaction parameters such as reaction time, reaction temperature, choice of solvent and

stoichiometry of the reactants [37]. Fig. S1 (a and b) shows the HR-TEM image and their

corresponding line profile map. The peak to peak average distance measured using the relation average distance/number of cycles [38], yield the value of 0.51 nm which is close to the *d*-spacing of (111) plane of the ferrite phase. Fig. S2 shows the selected area electron diffraction (SAED) pattern of sample A which exhibits bright spots arranged in rings indicating the polycrystalline nature which agreed well with XRD patterns and their corresponding crystallographic planes are indexed. Fig. 3 (b) and 3 (c) show the particle size distributions (PSD) of spherical and rhombohedron nanoparticles using the image analysis program ImageJ and the obtained histograms were fitted well with the Gaussian distribution. The average particle size of the spherical (diameter) and rhombohedral (width) nanoparticles was found to be 4.2 ± 1.3 and 27.5 ± 13.6 nm respectively.
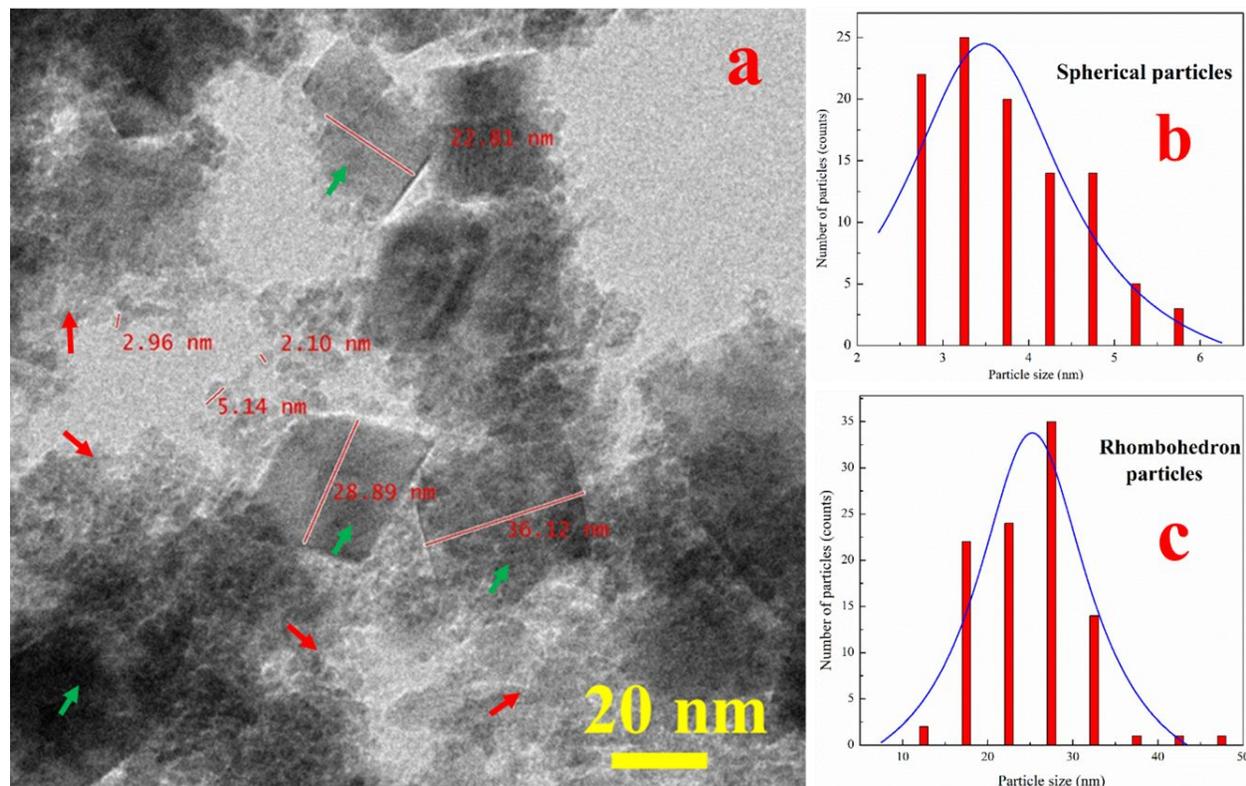
Fig. 3. (a) TEM images, and (b & c) particle size distribution of as prepared $CoFe_2O_4$ nanoparticles.

Fig. 4 (a) shows the TEM image of sample A ($CoFe_2O_4$) after heat treatment, which reveals round edged nearly rectangular shaped morphology. Before heat treatment of sample A, bimodal distribution of spherical and rhombohedral particles were observed which on heat treatment at 800 ºC transformed into nearly homogeneous particles. Fig 4 (b) shows the PSD along with Gaussian distribution of heat treated sample A and the average particle size was found to be 37.5 ± 13.69 nm. Fig. S3 (a and b) shows the HRTEM image and line profile map of heat treated sample. The peak to peak average distance is 0.52 nm which closely matches with the (111) plane for cobalt ferrite.
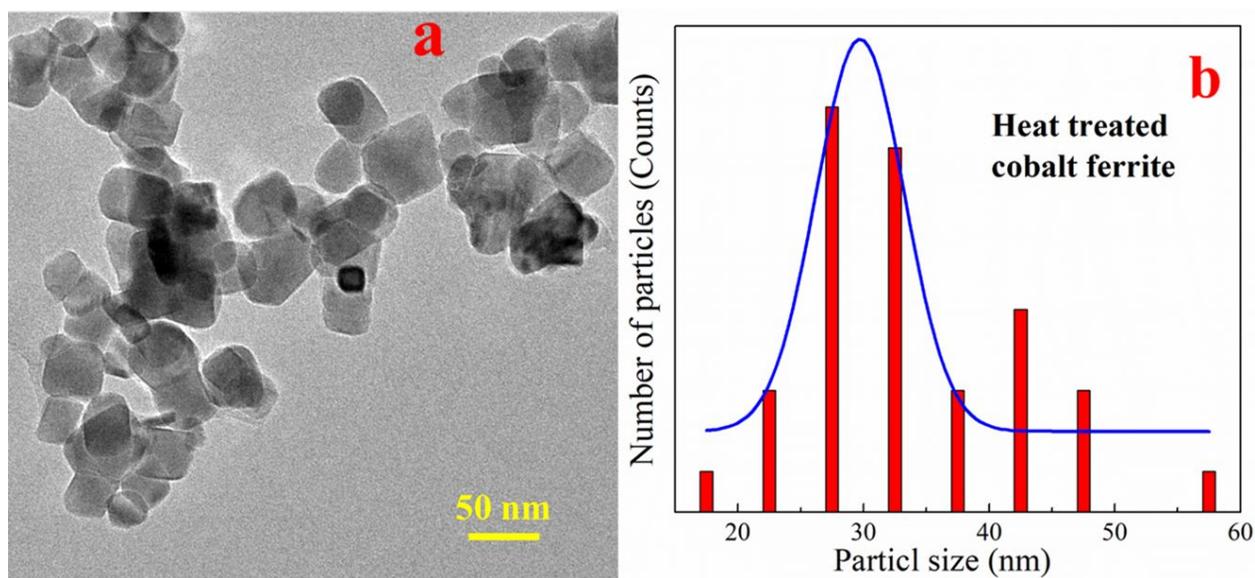
Fig. 4. (a) TEM image and (b) size distribution of the heat treated cobalt ferrite.

Fig. 5 (a) and 5 (b) show the morphology of sample B, as it can be observed from the image cobalt ferrite is found to be encased within HAp nanorods. The inset at the top right corner shows the magnified image revealing both the phases. However magnetic phase encasing within the nanorods is very random. Fig. S4 shows SAED pattern of sample B which exhibits bright spots arranged in rings indicating the polycrystalline nature of the sample which agreed well with XRD

patterns and crystallographic planes that corresponds to cobalt ferrite and HAp are indexed. PSD

of sample B obtained using image analysis program ImageJ is shown in Fig. 5 (c) along with

Gaussian distribution. Meanwhile, there are some particles which do not contain magnetic phase.

Fig S5 (a and b) shows the STEM image and elemental mapping of sample B.
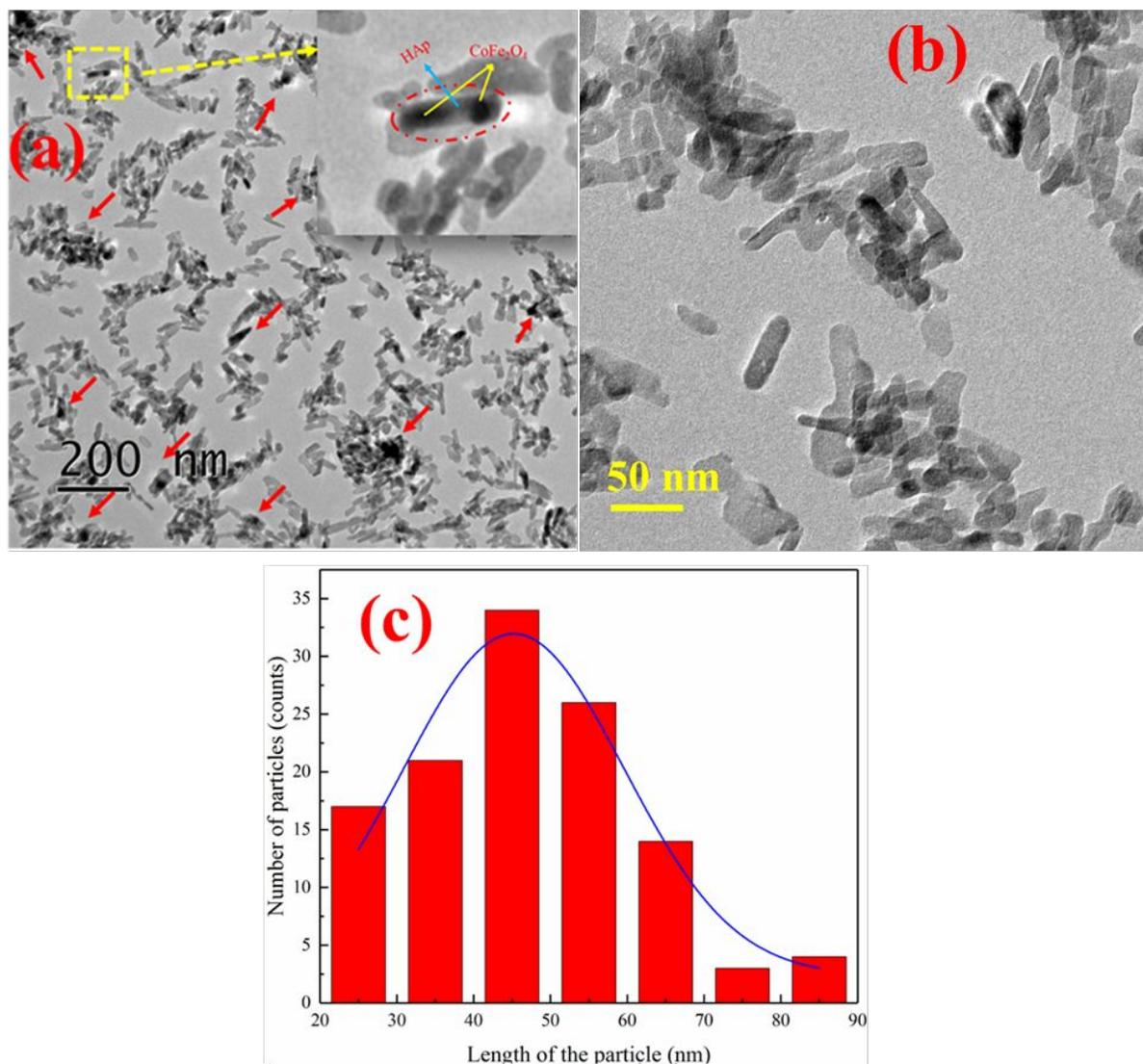
Fig. 5. (a and b) TEM images and (c) PSD of sample B.

On heat treatment the rod shaped cobalt ferrite encased HAp nanoparticles (sample B) has

changed into nearly spherical like core-shell structure (Fig. 6 a). During the heat treatment thermal

energy induced grain growth yielded dark inner cobalt ferrite core surrounded by nearly spherical like hydroxyapatite shell. Fig 6 (b) shows the thickness distribution of the shell over the core along with fitted Gaussian distribution curve. The average thickness of the shell was found to be 10 ± 4.89 nm. The magnetic core-shell $CoFe_2O_4@HAp$ particles can be separated magnetically, from Fig. 6 (c) we can see most of the particles are found to get attracted to the magnet (yellow arrow) and the remaining particles are settled down (green arrow). Fig. S6 (a) and (b) shows the STEM and elemental mapping of the sample C.
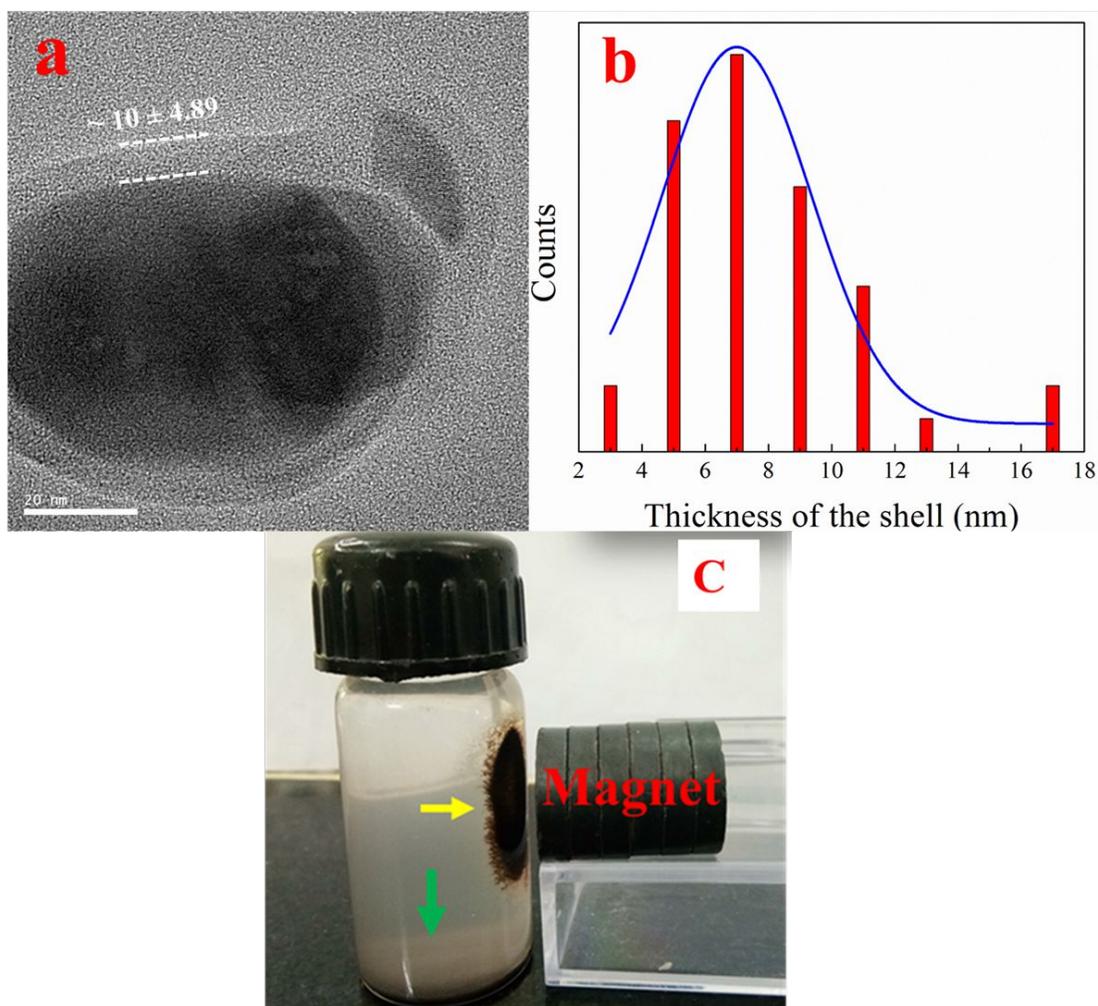
Fig. 6. (a) TEM image core-shell structured HAp@CoFe$_2$O$_4$, (b) shell thickness distribution of HAp and (c) magnetic separation of sample C.
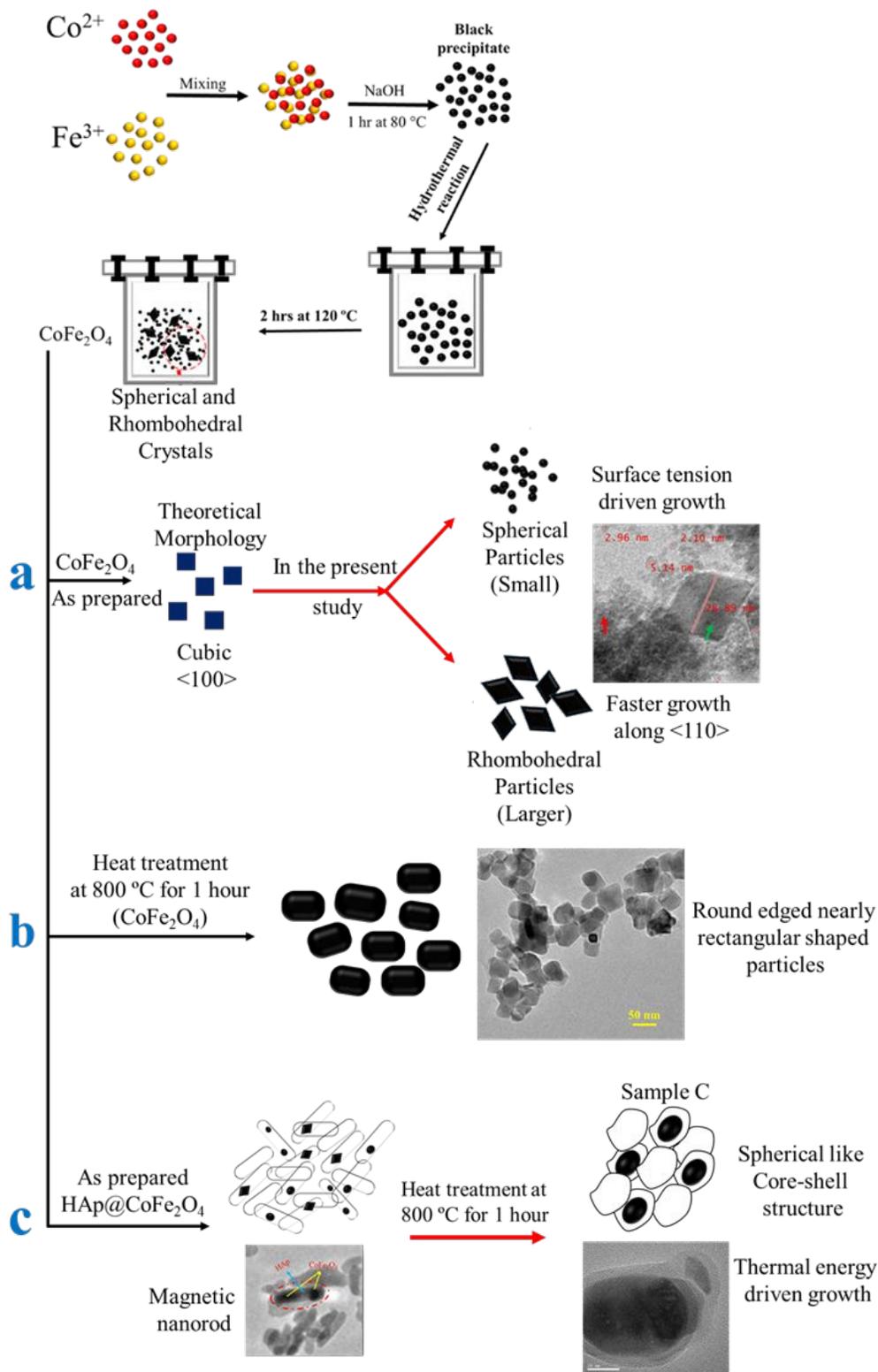
Fig. 7. Schematic illustration of the (a) possible growth mechanism of cobalt ferrite nanoparticle with two different habits, (b) cobalt ferrite after heat treatment and (c) transformation of magnetic nanorods into core-shell structure of HAp@CoFe$_2$O$_4$.

Coppola *et al.*, has reported the hydrothermal synthesis of Zn substituted cobalt ferrite nanoparticles having both spherical and octahedral/cubic structure [39]. Increase in particle size and transformation from spherical to cubic with increasing reaction time has been reported in the synthesis of nickel ferrite [40]. Formation of particles with diverse morphology and inhomogeneous size by the hydrothermal method may be due to incomplete particle growth. During the hydrothermal reaction formation of small spherical nanoparticles may take place initially and then grow into rhombohedral nanoparticle. Generally, cubic spinel structure should form crystals with cubic habits and/or habits reflecting growth along preferential axis. In the present work small sized spherical nanoparticles and relatively larger sized rhombohedral habits have been observed. Small nanoparticles tend to form a spherical shape because surface tension drives the nanoparticle growth towards spherical shape which corresponds to smallest surface area. In the case of larger particles faster growth along the preferred directions <110> from <100> tend to form rhombohedral particles [29,39]. Fig 7 (a) shows the schematic of the possible growth mechanism of cobalt ferrite nanoparticle with two different morphologies.

Fig 7 (b) shows the schematic of heat treated (at 800 °C for 1 hour) cobalt ferrite nanoparticles. The particles showed round edged rectangular shaped morphology along with grain growth. Because, during the heat treatment thermal energy drives the nanoparticle growth which yield homogeneity in PSD. Fig. 7 (c) shows the schematic of as formed HAp encased cobalt ferrite magnetic nanorods and formation of core-shell structure after heat treatment. HAp belongs to the hexagonal crystal system, during the synthesis HAp nanoparticles try to form a hexagonal crystal habit which reflects preferential growth along *c*-axis. This may be the reason for formation of rod like HAp@$CoFe_2O_4$ in the as prepared sample B. After heat treatment of sample B yielded core-shell structured magnetic particles.
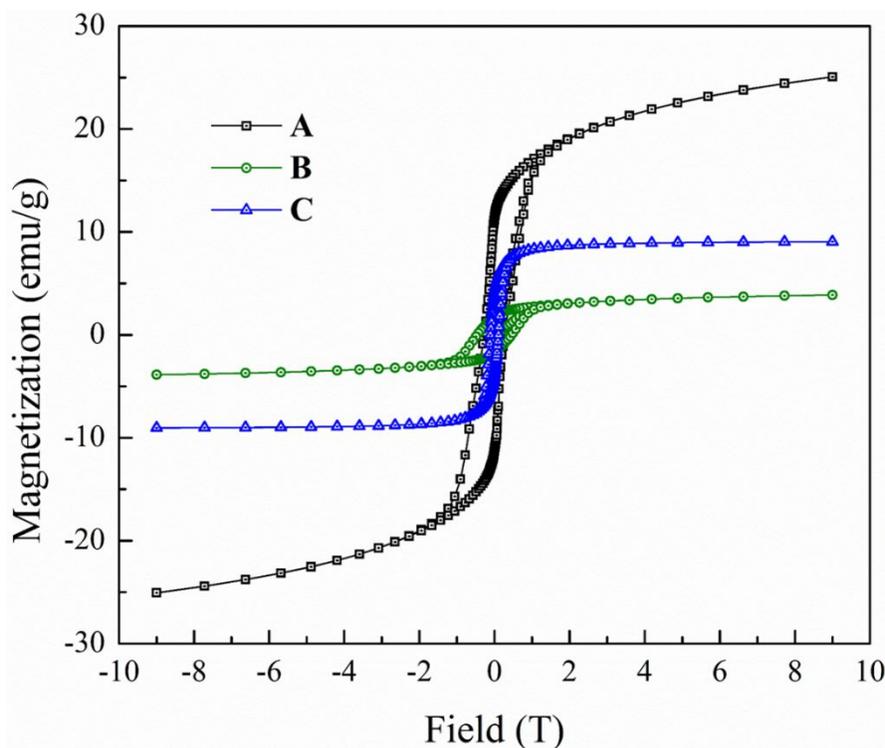
Fig. 8. M-H plots of the sample A (as prepared cobalt ferrite), B (as prepared coated sample) and C (heat treated coated sample) measured at $T = 300$ K.

Fig 8 shows the magnetization plots of the samples at room temperature (300 K), measured in the field range from -9 to +9 T. From the shape of the curves it is evident all the samples are ferromagnetic in nature at room temperature. Samples A, B, and C exhibited saturation magnetization (M_S) of 25, 3.77 and 9.04 emu/g with a coercivity of 0.26, 0.45 and 0.1 T, respectively. Since the magnetization values are evaluated using total weight of the sample ($CoFe_2O_4 + HAp$), it is considerably lower compared to pure $CoFe_2O_4$. The M_S of the sample A is less compared to that of the bulk cobalt ferrite (80 emu/g) [41]. This may be due to the inhomogeneity in particle size distribution that varies from 4.2 ± 1.3 nm (spherical) to 27.5 ± 13.6 nm (rombohedron) [Fig. 3 (a - c)], degree of cation inversion, size effect, surface effect, crystallinity and interparticle interaction are responsible for saturation magnetization of the

nanosized spinel ferrites. In nano regime, ferrite particles showed broken symmetry and exchange

bonds in its surface that caused the reduction of saturation magnetization when compared to bulk

[41]. While after heat treatment, sample A exhibited a saturation value *Ms* of 77.5 emu/g with

coercivity 0.116 T and the corresponding *M-H* curve is shown in Fig. 9. After heat treatment, *Ms*

of sample A enhanced significantly and is close to that of the bulk cobalt ferrite (80 emu/g) which

may be due to the increased crystallite size and nearly homogeneous PSD.

Bare $CoFe_2O_4$ (sample A) nanoparticles exhibited high saturation magnetization when

compared to coated samples. The diamagnetic behavior of the coating (HAp) has profoundly

affected the saturation magnetization of $CoFe_2O_4$. When compared to as prepared HAp coated

$CoFe_2O_4$ (sample B), the heat treated sample (C) showed higher saturation magnetization and

reduced coercivity due to the improved crystallinity of $CoFe_2O_4$ phase which is in agreement with

the published XRD results [42]. Table 2 shows the comparison of saturation magnetization of the

present study and previously reported values.

The magnetic moment of inverse spinel structured material such as cobalt ferrite $[(Fe^{3+})^A$

$(Co^{2+}, Fe^{3+})^B]$ depends on its cation distributions over the two sublattices (A-site and B-site).

Generally, the coupling between A and B-site moments are anti-parallel, hence the magnetic

moment of Fe^{3+} cancel out. The overall magnetic moment of cobalt ferrite unit cell depends on the

Co^{2+} cation and the magnetic moment of Co^{2+} is 3.87 μ_B per formula unit [27,43]. The calculated

value of the magnetic moment of the samples A, B and C using equation 3 is 1.05 μ_B, 0.15 μ_B and

0.37 μ_B respectively, which is much less than the expected value (3.87 μ_B). Various factors such

as distribution of cations, disorders in grains and grain size in the as prepared sample may be the

reason for this [43]. After heat treatment, the magnetic moment of A is 3.2 μ_B which is close to

the expected value. The enhancement in the magnetic moment of the coated sample is also obvious

from the values given in Table 3.
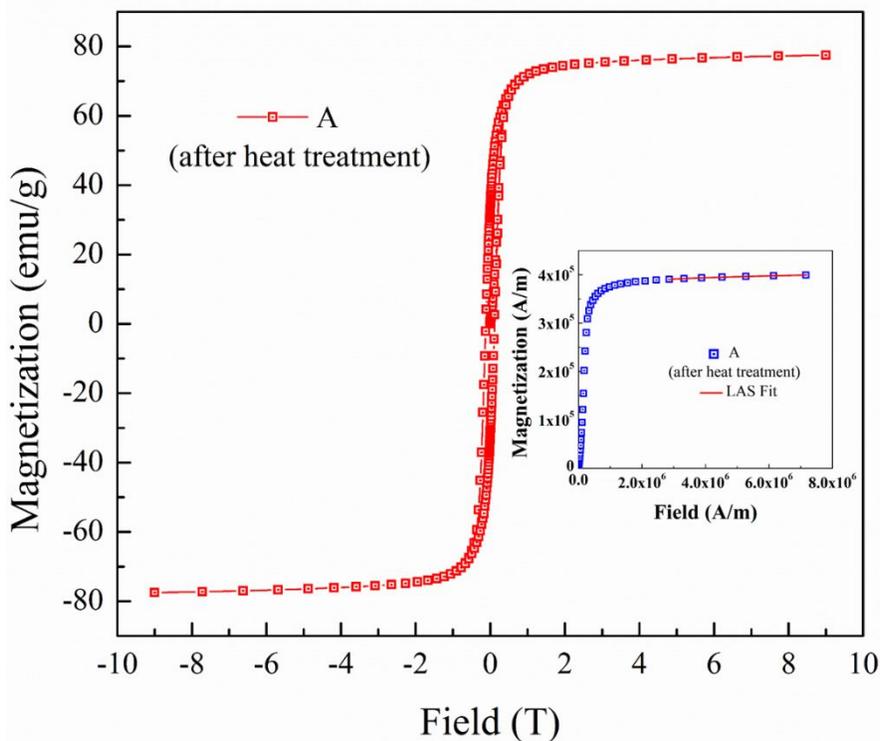
Fig. 9. M-H curve of the sample A after heat treatment at 800 °C for 1 hr. inset at the bottom right corresponding LAS fit.
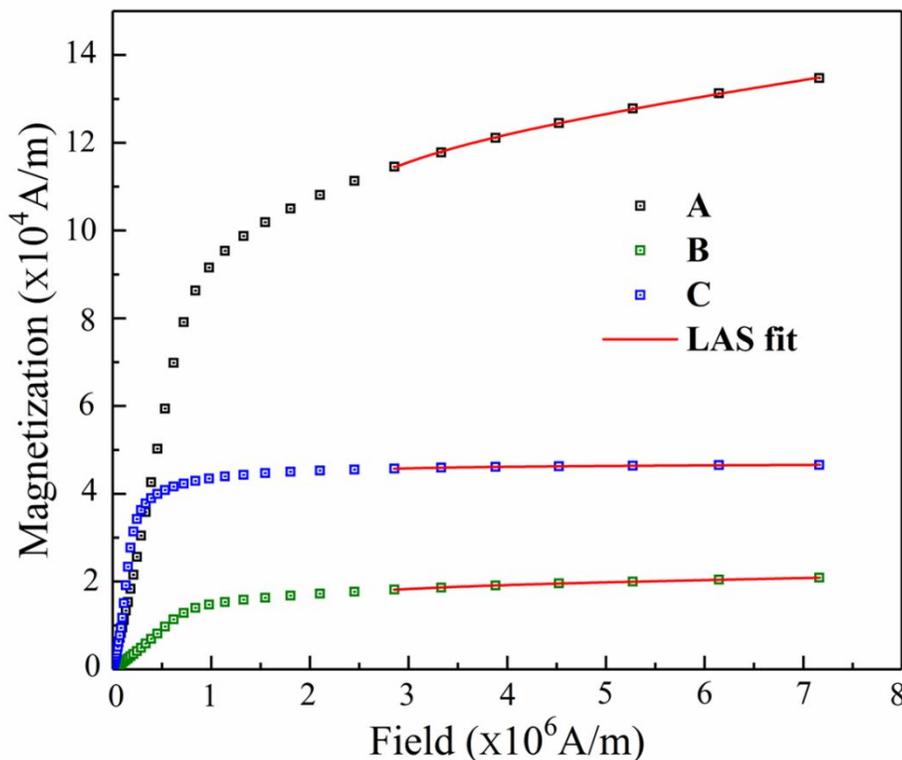
Fig. 10. LAS fit (see text for details) of synthesized samples A, B and C. Here the first quadrant of the magnetization ($T = 300\ K$) is plotted against magnetic field and the unit for the magnetic field is A/m.

The first order cubic magnetocrystalline anisotropy constant (K_1) of the synthesized samples was estimated using the law of approach to saturation (LAS) in the high field region using Eqn. 6. In order to fit our magnetization data to LAS expression, we have plotted the first quadrant of the magnetization versus magnetic field and the unit for the applied magnetic field is in A/m. Fig. 10 shows fitting of LAS equation for the synthesized samples A, B & C and the values of K_1 are $0.381 \times 10^6\ J/m^3$, $0.061 \times 10^6\ J/m^3$ and $0.076 \times 10^6\ J/m^3$ respectively. When compared to sample B, the magnetic anisotropy increased after heat treatment as seen in sample C. Magnetic anisotropy of the heat treated sample A is $0.501 \times 10^6\ J/m^3$, which is quite high when compared to sample A and the corresponding fitted curves is shown in the right inset of Fig. 9.

Cobalt ferrite is an inverse spinel structured material, which contains half of the Fe^{3+} cation in the tetrahedral A-site and remaining Fe^{3+} cations plus Co^{2+} cations in the octahedral B-site.

Generally, the magnetic properties such as saturation magnetization, coercivity, magnetic moment (m) and anisotropy constant (K) of the spinel structured materials depends on the distribution of cations in the A-site and B-site [27,44]. The distribution of cations in the A and B site may not be proper in the as prepared state. Heat treatment at appropriate temperature may redistribute the cations, leading to more Co^{2+} cations in A-site and more Fe^{3+} cation in B-site. If the spinel material is partially inverse (i.e., initially some Co^{2+} in A-site), then during heat treatment, the Co^{2+} cations would migrate towards the B-site resulting in the change in magnetic properties of cobalt ferrite [27,45].

Hence, the observed increase in saturation magnetization, magnetic moment and a decrease of coercivity of the heat treated samples can prima facie be attributed to the growth of crystallite and/or grain size and redistribution of cations in the spinel lattice of cobalt ferrite due to the heat treatment process. Similar kind of observation has been reported by Yadav et al. [46], where they observed increase in crystallite size and saturation magnetization up on heat treatment.. Furthermore, with the help of X-ray photoelectron spectroscopy the migration of Fe^{3+} ions from tetrahedral to octahedral site was also confirmed by them in addition to grain growth [46]. The strong magnetic anisotropy of cobalt ferrite is observed when Co^{2+} ion is in the B-site (inverse structured cobalt ferrite) [27]. Hence, increase of magnetic anisotropy in sample C and heat treated sample A represent, sample A has partial inverse structure initially, during the heat treatment A-site cobalt ions move towards the B-site, and this leads to increase the level of anisotropy, and it confirms the redistribution of cations over the spinel lattice.

Magnetic anisotropy is an intrinsic property of any magnetic material. The heat generating efficiency of the magnetic nanoparticle for magnetic hyperthermia depends on the magnetic anisotropy, saturation magnetization, particle size and distribution. Khurshid *et al.* [47], reported

the magnetic heating efficiency of the magnetic nanoparticles not only depends on its saturation

magnetization but also depends on the magnetic anisotropy. Tuning the magnetic anisotropy and

saturation magnetization in magnetic nanoparticle leads to an increase in the specific absorption

rate (SAR), which helps to decrease the therapeutic concentration of the magnetic nanoparticles

and attain a therapeutic temperature at a relatively shorter time [47,48]. Table 3 shows the

calculated magnetic parameters of the synthesized samples.

In addition, the magnetic particle size (magnetic domain size) was calculated using the

relation [49–51]:

$$d_{VSM} = \left[\frac{18\, k_B\, T}{\pi m_s} \sqrt{\frac{\chi_i}{3\, M_s H_0}} \right]^{\frac{1}{3}} \qquad (8)$$

where k_B is the Boltzmann constant (in erg/K), m_s is the saturation magnetization of the

bulk phase of cobalt ferrite which is 400 emu/cm^3 [49], M_s is the saturation magnetization of the

magnetic particles which is calculated by taking into account the density of cobalt ferrite for

sample A and for the heat treatment as 5.357 g/cm^3 and 5.151 g/cm^3, respectively. The saturation

moment for the sample A amounts to 25.06 emu/g in a field of 9 T and hence the saturation

magnetization M_s is thus estimated as 134.246 emu/cm^3, while that of the heat treated sample A is

estimated as 399.202 emu/cm^3. χ_i is the initial susceptibility, obtained from the slope of the low

field magnetization data, where the initial linear response was observed. H_0 is obtained from the

high field magnetization data. In order to obtain H_0, we plotted M vs. 1/H, and extrapolated the

high field magnetization data where it cuts the x-axis, namely here the (1/H) axis which yields the

H_0 value. The H_0 value thus obtained for sample A and the heat treated sample is (1/3.091x10^{-5}

Oe) and (1/3.363x10^{-5} Oe), respectively. Using these values we obtained the magnetic particle

size d_{VSM} as 1.86 nm for sample A and 2.044 nm for heat treated sample. Size of the small

spherical particles in sample A corresponds to calculated size. Hence, the small spherical particles

may be within the single domain superparamagnetic regime. After heat treatment the domain size

is increased slightly when compared to as prepared sample A. The heat treatment has essentially

increased the magnetic particle size. This is also evident from the relatively larger value of

magnetization when compared to as prepared sample A.

Table 2. Comparison of saturation magnetization of present study with reported value.

Materials	Saturation magnetization (emu/g)	Reference
Composite of $NiFe_2O_4$ along with HAp and β-TCP	1.15	[19]
Fe_3O_4-hydroxyapatite Nanocomposites	7.34	[52]
Co-ferrite – HAp	~5.20	[53]
CoFe2O4/HAP-modified wood composites	1.84	[54]
Hydroxyapatite encapsulated nano $CoFe_2O_4$	7.8	[55]
Co Fe_2O_4-hydroxyapatite nanocomposites	~8	[56]
Hydroxyapatite coated $CoFe_2O_4$	9.04	Present study

Table 3. Magnetic properties such as saturation magnetization, anisotropy constant and magnetic moment of the synthesized bare and coated nanoparticles at room temperature.

Samples Code	Saturation Magnetization obtained from M-H curve (emu/g)	First order magnetocrystalline anisotropy constant (K_1 10^6 J/m^3)	Magnetic moment per formula unit in μ_B
A	25.06	0.381	1.05
B	3.87	0.061	0.15
C	9.04	0.076	0.37
A (after heat treatment)	77.5	0.501	3.2

Fig. 11 shows the cell viability *vs* different dosage for the sample C with dosages - 50, 100, 200, 300 400 and 500 μg/ml. It is observed that even when incubated at high concentration (500 μg/ml) for 24 h, more than 76% of cells survived, which indicates the low cytotoxicity of the sample. Cell viability around 100% for concentration upto 400 μg/ml and survival of cells decreased to 76 % at high concentration (500 μg/ml). According to the biological evaluation of medical devices-part 5: tests for in vitro cytotoxicity (ISO 10993-5: 2009), if viability of the material is less than 70 % then it has a cytotoxic potential [57].
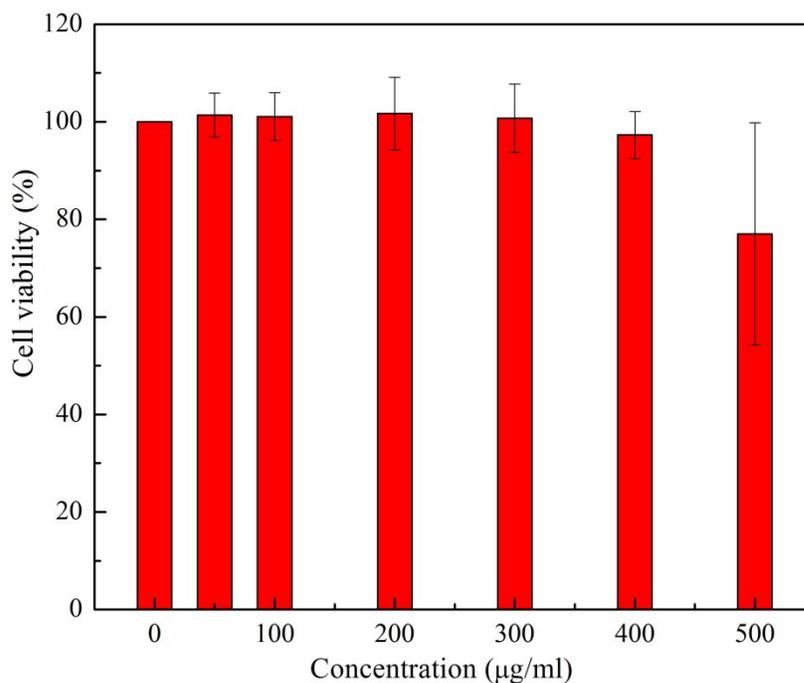
Fig. 11. Cytocompatibility of sample C with fibroblast 3T3 cells

4. Conclusions

Core-shell $CoFe_2O_4$@HAp magnetic nanoparticles were prepared by a simple two-step process using hydrothermal method. The morphology analyses using TEM observation clearly shows the encasing of $CoFe_2O_4$ within a rod-like hydroxyapatite and on heat treatment the a core-

24

shell nanostructure of $CoFe_2O_4@HAp$. All the synthesized samples exhibited ferromagnetic nature at room temperature. The saturation magnetization of heat treated samples got enhanced compared to the as coated sample due to the migration of cations in the spinel lattice and has been discussed based on the magnetic moment and magnetic anisotropy calculations. The MTT assay confirmed more than 76% cells survived even at high concentration (500 μg/ml) of core-shell magnetic particles which exhibits potential cytocompatibility of the sample.

Acknowledgements

Reference

[1]   I. Sharifi, H. Shokrollahi and S. Amiri, *J. Magn. Magn. Mater*., 2012, **324,** 903. doi:10.1016/j.jmmm.2011.10.017.

[2]   S. Mondal, P. Manivasagan, S. Bharathiraja, M.S. Moorthy, H.H. Kim, H. Seo, K.D. Lee and J. Oh, *Int J Nanomedicine.*, 2017, **12,** 8389. doi:10.2147/IJN.S147355.

[3]   N. Wu, D. Xu, Z. Wang, F. Wang, J. Liu, W. Liu, Q. Shao, H. Liu, Q. Gao, Z. Guo, *Carbon.,* 2019, **145**, 433. doi:10.1016/j.carbon.2019.01.028.

[4]   Y. Liu, N. Wu, Z. Wang, H. Cao and J. Liu. *New J. Chem.*, 2017,**41**, 6241. doi:10.1039/C7NJ00230K.

[5]   A. Baeza, D. Arcos and M. Vallet-Regí, *J. Phys. Condens. Matter*., 2013, **25**, 484003. doi:10.1088/0953-8984/25/48/484003.

[6]   Z. Nemati, J. Alonso, L.M. Martinez, H. Khurshid, E. Garaio, J.A. Garcia, M.H. Phan and H. Srikanth, *J. Phys. Chem*., C., 2016, **120,** 8370. doi:10.1021/acs.jpcc.6b01426.

[7]   Z. Nemati, S.M. Salili, J. Alonso, A. Ataie, R. Das, M.H. Phan and H. Srikanth, *J Alloy Compd*., 2017, **714,** 709. doi:10.1016/j.jallcom.2017.04.211.

[8]   Y.S. Sumithra, M.P. Kishore, B. Dhananjay and G.Virendra, *Nanomedicine (Lond).*, 2018, **13**, 1221.

[9]   A.H. Habib, C.L. Ondeck, P. Chaudhary, M.R. Bockstaller and M.E. Mchenry, *J. Appl. Phys.*, 2008, **103**, 07A307. doi:10.1063/1.2830975.

[10]   J. Robles, R. Das, M. Glassell, M.H. Phan and H. Srikanth, *AIP Adv.*, 2018, **8**, 056719. doi:10.1063/1.5007249.

[11]   C. Martinez-boubeta, K. Simeonidis, A. Makridis, M. Angelakeris, D. Serantes, D. Baldomir, Z. Saghi and P.A. Midgley, *Sci Rep.*, 2013, **3**, 1652. doi:10.1038/srep01652.

[12]   Z. Nemati, R. Das, J. Alonso, E. Clements, M.H. Phan and H. Srikanth. *J. Electron. Mater.*, 2017, **46**, 3764. doi:10.1007/s11664-017-5347-6.

[13]   M. Khramtsov, A. Garanina, P. Mogilnikov, N. Sviridenkova, I. Shchetinin, A. Savchenko, M. Abakumov and A. Majouga, *J. Magn. Magn. Mater.*, 2019, **469**, 443. doi:10.1016/j.jmmm.2018.09.014.

[14]   M. Sedlacik, V. Pavlinek, P. Peer and P. Filip, *Dalton Trans.*, 2014, **43**, 6919. doi:10.1039/c4dt00166d.

[15]   de la Vega, A.E., Garza-Navarro, M.A., Durán-Guerrero and J.G. et al. *J Nanopart Res.*, 2016, **18**, 18. doi:10.1007/s11051-016-3325-1.

[16]   G.S. Kumar, A. Thamizhavel, and E.K. Girija, *Mater. Lett.*, 2012, **76**, 198. doi:10.1016/j.matlet.2012.02.106.

[17]   A. Marques, Catarina Jose MF, Ferreira Ecaterina, Andronescu Ficai, Denisa Sonmez and Maria Ficai, *Int J Nanomedicine.*, 2014, **9**, 2713. doi.org/10.2147/IJN.S55943.

[18]   S. Karthi, G.A. Kumar, D.K. Sardar, G.C. Dannangoda, K.S. Martirosyan and E.K. Girija, *Mater. Chem. Phys.*, 2017, **193**, 356. doi:10.1016/j.matchemphys.2017.02.047.

[19]   R. Karunamoorthi, G. Suresh Kumar, A.I. Prasad, R.K. Vatsa, A. Thamizhavel and E.K. Girija, *J. Am. Ceram.*, Soc. 2014, **97**, 1115. doi:10.1111/jace.12746.

[20]   T. Ruthradevi, J. Akbar, G.S. Kumar, A. Thamizhavel, G.A. Kumar, R.K. Vatsa, G.C. Dannangoda, K.S. Martirosyan and E.K. Girija, *J Alloy Compd.*, 2017, **695**, 3211. doi:10.1016/j.jallcom.2016.11.300.

[21]   N. Wu, C. Liu, D. Xu, J. Liu, W. Liu, H. Liu, J. Zhang, W. Xie and Z. Guo. *J. Mater. Chem. C.*, 2019,**7**, 1659. doi:10.1039/C8TC04984J.

[22]   Y. Tang, X. Wang, Q. Zhang, Y. Lim and H. Wang, *Prog Nat Sci-Mater.*, 2012, **22**, 53. doi:10.1016/j.pnsc.2011.12.009.

[23] S. Singhal and K. Chandra, *J. Solid State Chem*., 2007, **180,** 296. doi:10.1016/j.jssc.2006.10.010.

[24] P.N. Anantharamaiah and P.A. Joy, *Phys. Chem. Chem. Phys*., 2016, **18**, 10516. doi:10.1039/c6cp00369a.

[25] A. Franco, Jr, F. L. A. Machado and V. S. Zapf, *J. Appl. Phys*., 2011, **110**, 053913. doi:10.1063/1.3626931.

[26]   A.C.Lima, M.A.Morales, J.H.Araújo, J.M.Soares, D.M.A.Melo and A.S.Carriçoa, *Ceram. Int*., 2015, **41**, 1. doi:10.1016/j.ceramint.2015.05.148.

[27] I.C. Nlebedim, N. Ranvah, P.I. Williams, Y. Melikhov, J.E. Snyder, A.J. Moses and D.C. Jiles, *J. Magn. Magn. Mater*., 2010, **322**, 1929. doi:10.1016/j.jmmm.2010.01.009.

[28] L. Kumar, P. Kumar, M. Kumar and Z. Manoranjan, *J Supercond Nov Magn.* 2017, **30,** 1629. doi:10.1007/s10948-016-3965-5.

[29] A. Lopez-Ortega, E. Lottini, C. J. Fernandez and C. Sangregorio, *Chem. Mater*., 2015, **27** 4048. doi:10.1021/acs.chemmater.5b01034.

[30] S. Prakash Parthiban, K. Elayaraja, E. K. Girija, Y. Yokogawa, R. Kesavamoorthy, M. Palanichamy, K. Asokan and S. Narayana Kalkura, *J Mater Sci: Mater Med*., 2009, **20**, S77. doi. 10.1007/s10856-008-3484-4.

[31] E.K. Girija, G.S. Kumar, A. Thamizhavel, Y. Yokogawa, S.N. Kalkura, *Powder Technol*., 2012, **225**, 190. doi:10.1016/j.powtec.2012.04.007.

[32] S. Rana, J. Philip and B. Raj, *Mater. Chem. Phys.,* 2010, **124**, 264. doi:10.1016/j.matchemphys.2010.06.029.

[33] P.N. Oliveira, D.M. Silva, G.S. Dias, I.A. Santos and L.F. Cótica, *Ferroelectrics*., 2016, **499** 76. doi:10.1080/00150193.2016.1172882.

[34] S. Kanagesan, M. Hashim, S. Tamilselvan, N.B. Alitheen, I. Ismail and G. Bahmanrokh, *J Nanomater*., 2013, **2013**, 1. doi:10.1155/2013/865024.

[35] T. Boobalan, N. Suriyanarayanan and S. Pavithradevi, *Mat Sci Semicon Proc*., 2013, **16**, 1695. doi:10.1016/j.mssp.2013.04.013.

[36] G.S. Kumar, S. Rajendran, S. Karthi, R. Govindan, E.K. Girija, G. Karunakaran and D. Kuznetsov, *MRS Commun*., 2017, **7**, 183. doi:10.1557/mrc.2017.18.

[37] J.A. Darr, J. Zhang, N.M. Makwana and X. Weng, *Chem. Rev*. 2017, **117**, 11125. doi:10.1021/acs.chemrev.6b00417.

[38] G. Fu, Y. Chen, Z. Cui, Y. Li, S. Xin, Y. Tang, J.B. Goodenough, *Nano Lett.*, 2016, **16**,

6516. doi:10.1021/acs.nanolett.6b03133.

[39] P.F.G. Coppola, S.G. Gomide, A.F.C.C.R. Perzynski and C.K.J. Depeyrot, *J. Nanoparticle Res.,* 2016, **18**, 1. doi:10.1007/s11051-016-3430-1.

[40] Z. Ying, R. Gaurab, T. Jinke and D. Qilin, *Mater. Res. Express.,* 2018, **5**, 025023. doi. 10.1088/2053-1591/aaacde.

[41] K. Maaz, M. Usman, S. Karim, A. Mumtaz, S.K. Hasanain and M.F. Bertino, *J. Appl. Phys*., 2009, **105**, 113917. doi:10.1063/1.3139293.

[42] C.H. Chia, S. Zakaria, M. Yusoff, S.C. Goh and C.Y. Haw, *Ceram Int*., 2010, **36**, 605. doi:10.1016/j.ceramint.2009.10.001.

[43] R.B. Kamble, V. Varade, K.P. Ramesh, V. Prasad, R.B. Kamble, V. Varade, K.P. Ramesh and V. Prasad, *AIP Adv*., 2015, **5**, 017119. doi:10.1063/1.4906101.

[44] J.G. Na, T.D. Lee and S.J. Park, *J. Mater. Sci. Lett*., 1993, **12**, 961. Doi. 10.1007/BF00455632

[45] J.G. Na, T.D. Lee, S.J. Park, Y.J. Tang and H.L. Luo, *Ieee Trans. Magn*., 1995, **31**, 3970. doi. 10.1109/20.489833.

[46] R.S. Yadav, I. Kuřitka, J. Vilcakova, J. Havlica, J. Masilko, L. Kalina, J. Tkacz, J. Švec, V. Enev and M. Hajdúchová, *Adv. Nat. Sci: Nanosci. Nanotechnol*., 2017, **8**, 045002.

[47] H. Khurshid, J. Alonso, Z. Nemati, M.H. Phan, P. Mukherjee, M.L. Fdez-Gubieda, J.M. Barandiarán and H. Srikanth, *J. Appl. Phys*., 2015, **117**, 17A337. doi:10.1063/1.4919250.

[48] T. Yadavalli, H. Jain, G. Chandrasekharan and R. Chennakesavulu, *AIP Adv*, 2016, **6**, 055904. doi:10.1063/1.4942951.

[49] O. Karaagac, H. Kockar, S. Beyaz, and T. Tanrisever, *IEEE Trans. Magn*., 2010, **46**, 12. doi.10.1109/TMAG.2010.2076824.

[50] O. Karaagac, B. B. Yildiz and H. Köçkar, *J. Magn. Magn. Mater.,* 2019, **473**, 262. doi:10.1016/j.jmmm.2018.10.063.

[51] M. P. Morales, S. Veintemillas-Verdaguer, M. I. Montero, and C. J. Serna, *Chem. Mater*., 1999, **11**, 3058-3064. doi:10.1021/cm991018f.

[52] M. Sneha and N.M. Sundaram, *Int. J. Nanomedicine.*, 2015, **10**, 99. doi.10.2147/IJN.S79985.

[53] N. Petchsang, W. Pon-On, J.H. Hodak and I.M. Tang, *J. Magn. Magn. Mater.*, 2009, **321,** 1990. doi:10.1016/j.jmmm.2008.12.027.

[54] W. Gan, L. Gao, X. Zhan and J. Li, *RSC Adv.*, 2015, **5**, 45919. doi:10.1039/C5RA06138E.

[55] F. Foroughi, S.A. Hassanzadeh-Tabrizi and J. Amighian, *J. Magn. Magn. Mater.* 2015, **382,** 182. doi:10.1016/j.jmmm.2015.01.075.

[56] K. Sangeetha, M. Ashok and E.K. Girija, *Ceram Int.*, 2019, **45**, 12860. doi:10.1016/j.ceramint.2019.03.209.

[57] http://www.iso.org/iso/home.html

GRAPHICAL ABSTRACT